Photocatalysis

DOI: 10.1002/anie.201406638

Direct Imaging of Light Emission Centers in Two-Dimensional Crystals and Their Luminescence and Photocatalytic Properties**

Shintaro Ida, Shota Koga, Takeshi Daio, Hidehisa Hagiwara, and Tatsumi Ishihara*

Abstract: *To fully understand the fundamental properties of light-energy-converting materials, it is important to determine the local atomic configuration of photofunctional centers. In this study, direct imaging of one- and two-Tb-atom emission centers in a two-dimensional Tb-doped $Ca_2Ta_3O_{10}$ nanocrystal was carried. The emission centers were located at the Ca sites in the perovskite structure, and no concentration-based quenching was observed even when the emission centers were in close proximity to each other. The relative photoluminescence efficiency for green emission of the nanosheet suspension was 38.1 %. Furthermore, the Tb-doped $Ca_2Ta_3O_{10}$ nanocrystal deposited co-catalyst showed high photocatalytic activity for hydrogen production from water (quantum efficiency: 71 % at 270 nm). Tb^{3+} dopants in the two-dimensional crystal might have the potential to stabilize the charge separation state.*

Light-energy-converting materials play a crucial role in many types of energy-saving devices[1] and for renewable energy technology.[2] Among the most important research goals for luminescent materials are developing long-lived materials that exhibit high brightness, and achieving accurate control over luminescence properties such as the color tone and excitation wavelength. Luminescent materials are often prepared by doping inorganic crystals to produce emission centers.[3,4] However, one issue associated with such doping is the phenomenon of concentration-based quenching, which decreases the luminescence intensity with increasing dopant concentration. The precise reason for this has still not been determined, although an increase in the proximity of emission centers and the formation of emission-center clusters have both been proposed.[5–7] Photocatalytic hydrogen production from water is certainly seen as one of the key players in renewable energy systems based solely on water and solar energy.[2] A method to improve the catalytic activity is doping with transition metals,[8,9] where the transition-metal doping is performed to control the concentration of electrons and/or to improve the response to visible light. However, the actual role of the dopant in the photocatalyst material is still under discussion. One of the best ways to resolve these issues would be to carry out direct observations of individual photofunctional centers in luminescent materials.[10] Although direct scanning transmission electron microscopy (TEM) observations of dopant atoms has been reported, complicated calculations and observation methods are necessary to obtain a clear one-atom dopant image.[11] In general, it is difficult to rigorously determine whether one or more dopant atoms are present along the electron-beam path, because it is difficult to estimate the atomic number in this direction.

Recently, two-dimensional oxide crystals (nanosheets) with photoluminescence characteristics have been reported.[12] The nanosheets are prepared by exfoliation of layered compounds, and have a uniform thickness. For example, the thickness of perovskite $A_2B_3O_{10}$ (A: Ca, Sr, Ba, B: Nb, Ta) nanosheets corresponds to the length of three BO_6 octahedral units.[13] Such nanosheets with a homogeneous ultrathin thickness are suitable host crystals for studying emission centers produced by doping. We previously reported that Rh-doped $Ca_2Nb_3O_{10}$ nanosheets exhibited a high photocatalytic activity for hydrogen production from water, without the need of cocatalyst loading, and it was considered that the reaction centers were associated with single Rh atoms.[14] However, there have been no reports on direct observations of single dopant atoms in photocatalysts. Therefore, direct TEM observations of the environment of dopant atoms may provide insights that prove useful in several research fields. In the present study, we report direct observations of dopant atoms acting as emission centers in green-emitting Tb-doped $Ca_2Ta_3O_{10}$ nanosheets, and its unusual photoluminescence and photocatalytic properties.

Tb^{3+}-doped $Ca_2Ta_3O_{10}$ nanosheets were prepared by exfoliation of $CsCa_{(2-x)}Tb_xTa_3O_{10}$. The $CsCa_{(2-x)}Tb_xTa_3O_{10}$ was prepared using a conventional solid-state reaction. It can be seen that in the range $x = 0.001$–0.1, all of the XRD patterns look the same (see Figure S1 in the Supporting Information), and are similar to that previously determined for tetragonal $CsCa_2Ta_3O_{10}$ (space group P4/mmm) with lattice parameters of $a = b = 3.8659(1)$ and $c = 15.2538(5)$ nm (ICSD number 89011).[15] It is possible for Tb^{3+} to occupy Ca^{2+} sites (A sites) in the lattice. Although

[*] Prof. S. Ida
International Research Center for Hydrogen Energy
Department of Applied Chemistry, Faculty of Engineering
Kyushu University
744 Motooka, Nishi-ku, Fukuoka 819-0395 (Japan)
and
PRESTO (Japan) Science and Technology Agency (JST)
4-1-8 Honcho Kawaguchi, Saitama 332-0012 (Japan)
E-mail: s-ida@cstf.kyushu-u.ac.jp

S. Koga, Prof. H. Hagiwara, Prof. T. Ishihara
International Research Center for Hydrogen Energy
Department of Applied Chemistry, Faculty of Engineering
Kyushu University
744 Motooka, Nishi-ku, Fukuoka 819-0395 (Japan)

T. Daio
International Research Center for Hydrogen Energy
Kyushu University
744 Motooka, Nishi-ku, Fukuoka 819-0395 (Japan)

[**] This research was supported by JST, PRESTO and JSPS KAKENHI 24685031.

Supporting information for this article is available on the WWW under http://dx.doi.org/10.1002/anie.201406638.

such substitution might be expected to lead to peak shifts in the XRD pattern, no obvious peak shift was apparent in the XRD pattern (Figures S2 and S3). In the case of $CsCa_{(2-x)}Tb_xTa_3O_{10}$ ($x = 0.2$), an impurity phase was observed in the XRD pattern. Therefore, all subsequent experiments were performed on materials with $x = 0$–0.100.

Exfoliation of the bulk layered oxide to single nanosheets was confirmed by atomic force microscopy observations. Figure 1 shows the AFM image of $Ca_{2-x}Tb_xTa_3O_{10}$ ($x = 0.1$) nanosheet, cross sectional profile of the AFM image, and

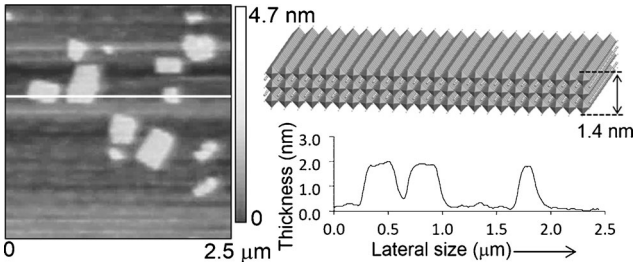

Figure 1. AFM image of the $Ca_{2-x}Tb_xTa_3O_{10}$ ($x = 0.1$) nanosheet, cross-sectional profile of the AFM image, and structure model of a single nanosheet.

structure model of mono nanosheet. The nanosheets were approximately 1.5–1.7 nm thick, which corresponded to the theoretical value. Figure 2a shows a 200 kV high-angle annular dark-field scanning transmission electron microscopy (HAADF-STEM) image of a $Ca_{2-x}Tb_xTa_3O_{10}$ ($x = 0.1$) nanosheet. The HAADF detector collects electrons that undergo high-angle scattering, and the signal intensity is approximately proportional to Z^2, where Z is the atomic number. Thus, the HAADF technique is more sensitive to heavy atoms, and Ta ($Z = 73$) and Tb ($Z = 65$) ions are clearly seen in the HAADF image. Since there are three B sites (Ta) and two A sites (Ca or Tb) in the nanosheet along the electron beam direction, the brightest spots represent three Ta atoms at B sites, the spots with intermediate brightness represent two Tb atoms at A sites, and the darkest spots represent a single Tb atom at an A site. Because of the low atomic number ($Z = 20$), Ca atoms at A sites are not visible in the image. Figure 2b shows a color-coded intensity map derived from Figure 2a, where the contrast was adjusted to highlight the dopant atoms, which are indicated by arrows in the image. The angle between the *a* axis and *b* axis was not 90°, which is due to drift effect. The density of the Tb atoms observed corresponded to the value expected for the doped amount x (Figures S5 and S6). Figure 2c shows the intensity profile along the line X to X' in Figure 2a. Point "S" in the line profile of Figure 2c represents a single A site doped with a Tb^{3+} ion, and point "T" represents two A sites doped with a Tb^{3+} ion. Figure 2d shows normalized intensity profiles for A sites containing 0, 1 or 2 Tb^{3+} ions. Thus, in the case of the $Ca_{2-x}Tb_xTa_3O_{10}$ nanosheet, it is easy to determine whether one or more dopant atoms are present along the electron-beam path, because it is possible to estimate the atomic number in this direction. The HAADF image simulation was carried out using the frozen phonon model with a 200 kV probe to

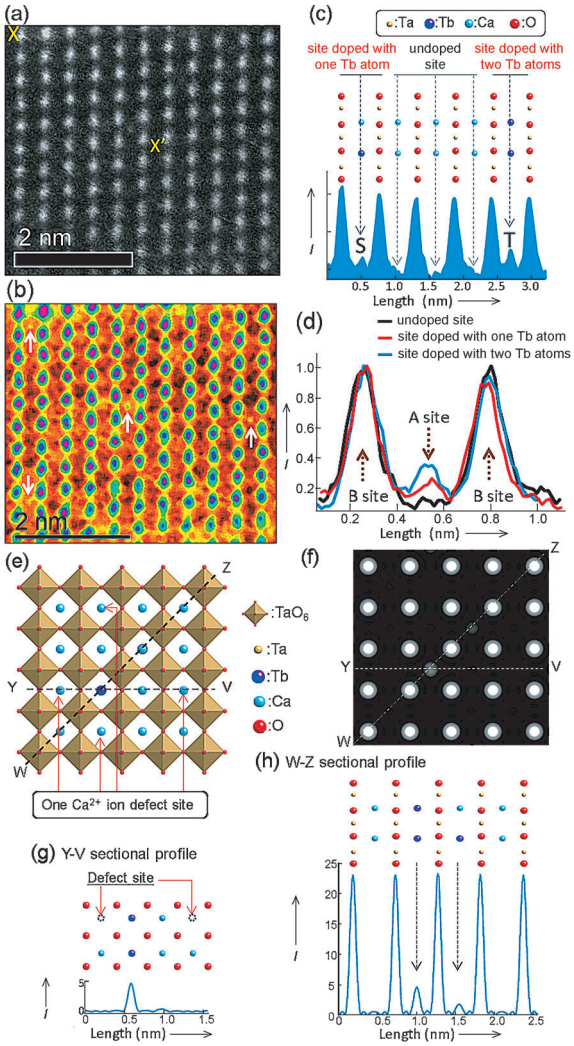

Figure 2. a) HAADF-STEM image of a $Ca_{2-x}Tb_xTa_3O_{10}$ ($x = 0.1$) nanosheet, b) color-coded intensity map derived from Figure 2a, c) structural model of the cross-sectional profile and the intensity profile along the line X to X' in Figure 2a, d) normalized intensity profiles for A sites containing 0, 1 or 2 Tb^{3+} ions, e) structural model for image simulation, f) HAADF image obtained by simulation, g) structural model of the cross-sectional profile and intensity profile along the line Y to V, and h) intensity profile along the line W to Z

quantitatively interpret the HAADF image. Figure 2e shows a model structure for image simulation, which has some defect sites in the A site to compensate the charge, since the Tb^{3+} ions are doped in the Ca^{2+} site. Figure 2f shows a HAADF image obtained by simulation. The brightest spots represent three Ta atoms at B sites, the spots with intermediate brightness represent two Tb atoms at A sites, and the darkest spots represent a single Tb atom at an A site. The HAADF image obtained by simulation agreed well with the actual HAADF image of the Tb-doped $Ca_2Ta_3O_{10}$ nanosheet. Figure 2g,h shows the intensity profiles along the lines Y to V and W to Z in Figure 2f, respectively. The intensity ratios for A-site(Tb)/B-site(Ta) obtained by simulation (Figure 2h) were slightly different from the actual ratio. This might be due to the TBA^+ ions adsorbed on the nanosheet and carbon grid for TEM measurement.

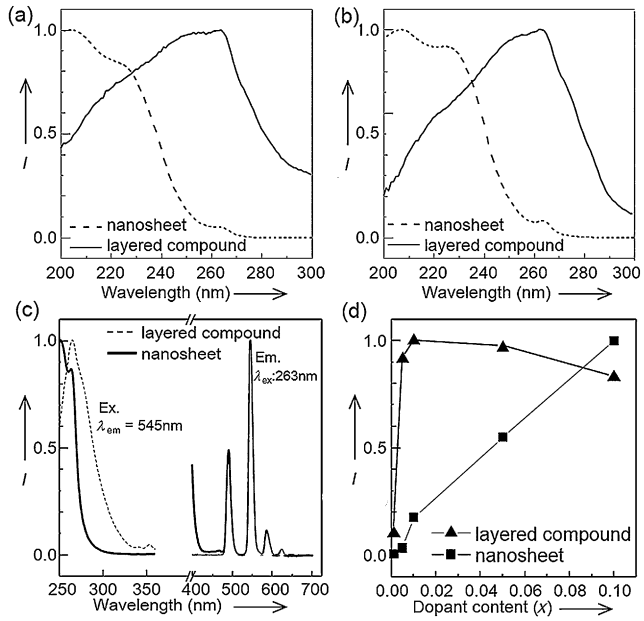

Figure 3. UV/Vis absorption spectra of $CsCa_{2-x}Ta_3O_{10}$ and its nanosheet for x = a) 0.005 and b) 0.100, and c) photoluminescence spectra for bulk layered $CsCa_{2-x}Tb_xTa_3O_{10}$ ($x = 0.1$) and $Ca_{2-x}Tb_xTa_3O_{10}$ ($x = 0.1$) nanosheet suspensions, and d) emission intensity ($\lambda_{em} = 545$ nm) for bulk $CsCa_{2-x}Tb_xTa_3O_{10}$ and the corresponding nanosheets as a function of the dopant content (solvent: 0.025 M TBAOH aqueous solution).

Figure 3 shows UV/Vis absorption spectra of $CsCa_{2-x}Tb_xTa_3O_{10}$ and its nanosheet for $x = 0.005$ and 0.100. The absorption edges of the layered compounds were at around 290–300 nm. When the layered compounds were exfoliated into nanosheets, the absorption edges were blue-shifted (260 nm) relative to the layered compounds (290–300 nm). This is attributed to a quantum size effect in the nanosheet. In addition, in the case of a nanosheet, a small absorption band was observed at 265 nm, which might corresponded to f–f or f–d transitions of Tb^{3+} in the nanosheet. The intensity of the absorption peak (265 nm) for $x = 0.1$ was larger than that for $x = 0.005$. This might be due to the amount of Tb^{3+} in the nanosheet. Figure 3c shows typical photoluminescence spectra for bulk layered $CsCa_{2-x}Tb_xTa_3O_{10}$ and its nanosheet suspensions. The maximum emission intensities are normalized to unity to allow an easy comparison. In reality, the maximum emission intensity ($x = 0.1$) was 48 times higher for the bulk compound, since the nanosheet concentration in the suspension was low. The emission peaks at 492, 545, 587, and 624 nm are assigned to $^5D_4$–^7F_j (j = 3-6) transitions of Tb^{3+}. In the excitation spectra for the bulk compound, a broad peak is observed at about 250–300 nm, which corresponds to the UV/Vis absorption spectra. This peak can be partially assigned to energy transfer from the bandgap excitation energy to Tb^{3+} in the host layer or the nanosheet. In the spectra for the nanosheets, one sharp peak is present at 263 nm, and might be assigned to f–f or f–d transitions of Tb^{3+}. Figure 3d shows the emission intensity ($\lambda_{em} = 545$ nm) for bulk $CsCa_{2-x}Tb_xTa_3O_{10}$ and the corresponding nanosheets as a function of the dopant content. The maximum intensity is normalized to unity. In the case of the bulk compound, the emission intensity reaches a maximum at $x = 0.01$, and decreases at higher dopant content because of concentration-based quenching. On the other hand, the emission intensity for the nanosheets increases monotonically with dopant content, indicating that no concentration-based quenching occurred up to $x = 0.10$. The TEM results indicate that some Tb^{3+} emission centers in the nanosheet ($x = 0.1$) exist in close proximity to each other as shown in Figure 2b and Figure S6. Despite this, no concentration-based quenching was observed, as was the case in the bulk parent compound for the same dopant content of $x = 0.1$ (Figure 3d). When the nanosheets were re-stacked into layered compound ($Cs/Ca_{2-x}Tb_xTa_3O_{10}$) by electrostatic self- assembly deposition reaction with Cs^+ ions, the concentration-based quenching was re-observed (Figure S7). These results imply that the non-radiative decay has structural anisotropic energy passes, which might be affected by the difference in the periodicity of the structure, and tends to occur preferably in the through-plane direction than in the in-plane direction of the nanosheet.

Figure 4a,b shows streak camera images of $CsCa_{2-x}Tb_xTa_3O_{10}$ and its nanosheet ($x = 0.100$). Four emission bands were observed, which were attributed to Tb^{3+} emissions with long emission lifetime (the y axis is millisecond time scale). In the case of the nanosheet, a broad emission band at around 400–650 nm with lifetime of microsecond scale was observed. Thus, it was found that the emission from the nanosheet contains sharp Tb^{3+} emissions with long lifetime and a broad emission with short lifetime. Figure 4c,d shows the emission decay curves for Tb^{3+} emission. The emission lifetime of the nanosheets was two times longer than that of the layered compounds. One reason for this could be that layered structure is changed to nanosheets by exfoliation reaction. This result also indicates that non-radiative decay is dependent on the crystal structure.

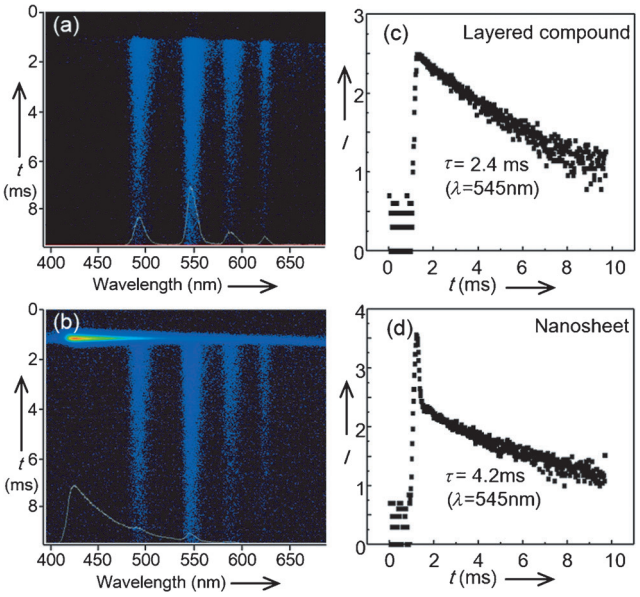

Figure 4. Streak camera images of a) $CsCa_{2-x}Tb_xTa_3O_{10}$ ($x = 0.100$) and b) $Ca_{2-x}Tb_xTa_3O_{10}$ nanosheet ($x = 0.100$), ($\lambda_{ex} = 266$ nm), and emission decay curves ($\lambda_{ex} = 266$ nm, $\lambda_{em} = 545$ nm) for c) $CsCa_{2-x}Tb_xTa_3O_{10}$ ($x = 0.100$) and d) $Ca_{2-x}Tb_xTa_3O_{10}$ nanosheet ($x = 0.100$).

Figure 5a show apparent quantum efficiency for photocatalytic hydrogen and photoluminescence efficiencies of $Ca_{2-x}Tb_xTa_3O_{10}$ nanosheets without co-catalyst loading in the presence of sacrificial agent (CH_3OH) as a function of the amount of doping with Tb^{3+}. The efficiency of the hydrogen production decreased from 19 to 8% with increasing amount of dopant. On the other hand, the photoluminescence efficiency increased from 4 to 38% with increasing the amount of dopant. In the presence of Tb^{3+}, the energy generated by photo-excitation was used not only for a photocatalytic reaction, but also for the photoluminescence of Tb^{3+}. Thus, it makes sense that photocatalytic activity decreased with increasing the doping amount of Tb^{3+}. Figure 5b shows apparent quantum efficiency for photocatalytic hydrogen and emission efficiencies of Rh-loaded (co-catalyst) $Ca_{2-x}Tb_xTa_3O_{10}$ sheets. The efficiency for the hydrogen production increased from 42 to 71% with increasing the amount of dopant from $x=0$ to 0.005, and decreased with increasing the amount of dopant from $x=0.005$ to 0.1. On the other hand, photoluminescence efficiency increased from 1 to 9% with an increasing amount of dopant. It is a reasonable result that the photocatalytic activity of Rh-loaded nanosheets was higher than that of nanosheets without co-catalyst loading, and that photoluminescence efficiency of Rh-loaded nanosheets was lower than that of a nanosheet without co-catalyst loading. However, Rh-loaded $Ca_{2-x}Tb_xTa_3O_{10}$ ($x=0.005$) nanosheets showed higher catalytic activity than the Rh-loaded $Ca_2Ta_3O_{10}$ nanosheet (undoped nanosheet), which is an unusual result. In general, it is expected that the activity of the Rh-loaded $Ca_{2-x}Tb_xTa_3O_{10}$ ($x=0.005$) nanosheets is lower than that of the Rh-loaded $Ca_2Ta_3O_{10}$ nanosheet (undoped nanosheet), since the Tb^{3+} ion (emission center) drains the photoexcited energy out of the photocatalyst. On the other hand, the photoluminescence lifetime of Tb^{3+} emission is longer than 1 ms as shown in Figure 5d. Perhaps, the photo-excited electrons or holes might be temporarily captured by Tb^{3+} ions, and then released for use in the photocatalytic reaction. The efficiency for the hydrogen production of La^{3+}-(non-luminescent ion-) doped $Ca_{2-x}La_xTa_3O_{10}$ ($x=0.005$) nanosheet was 35.4%, which was lower than that of the Tb-doped nanosheet (Figure S8). Thus, the Tb^{3+} dopant in the present nanosheet might have the potential to stabilize the charge separation state.

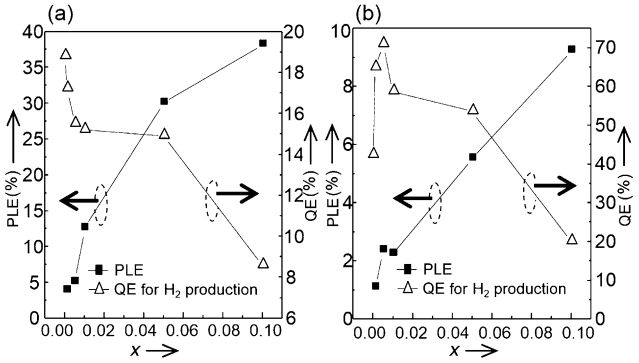

Figure 5. Apparent quantum efficiency (QE) for photocatalytic hydrogen (irradiation wavelength: 270 nm) and photoluminescence efficiencies (PLEs; $\lambda_{ex}=270$ nm) in aqueous 20 vol% methanol solution as a function of the amount of Tb^{3+} doping for a) $Ca_{2-x}Tb_xTa_3O_{10}$ nanosheets without co-catalyst loading and b) Rh(0.1 wt%)-loaded $Ca_{2-x}Tb_xTa_3O_{10}$ nanosheets.

In conclusion, the presence of one- and two-Tb-atom emission centers was confirmed in a two-dimensional $Ca_{2-x}Tb_xTa_3O_{10}$ nanocrystal. Some Tb^{3+} emission centers in the nanosheet existed in close proximity to each other. Despite this, no concentration-based quenching was observed, as was the case in the bulk parent compound for the same dopant content of $x=0.1$. This implies that the two-dimensional nature of the nanosheets affects the concentration-based quenching. These results might imply that the non-radiative decay has structural anisotropic energy passes. Furthermore, the Tb^{3+} dopant showed a positive effect for the photocatalytic activity. In general, the Tb^{3+}-doped photocatalyst is lower than that of undoped photocatalyst, since the emission center drains the photo-excited energy out of the photocatalyst. However, $Ca_{2-x}Tb_xTa_3O_{10}$ ($x=0.005$) nanosheets showed higher catalytic activity than undoped nanosheet. This indicates that the Tb^{3+} dopant in the nanosheet works as a photofunctional center for not only light emission, but it also decreases the recombination reaction rate.

Experimental Section

Tb^{3+}-doped $Ca_2Ta_3O_{10}$ nanosheets were prepared by exfoliation of $CsCa_{(2-x)}Tb_xTa_3O_{10}$ (experimental details: see the Supporting Information). High-angle annular dark-field scanning transmission electron microscopy (HAADF-STEM) images were obtained using a JEM-ARM200F microscope. HAADF image was simulated using Mac TempsX. The relative photoluminescence efficiencies of the nanosheet solution were estimated by comparison with solutions of quinine in aqueous 0.5 M H_2SO_4. A photocatalytic reaction was performed using a conventional closed circulation system. The nanosheet suspension (15 mL) containing 12 mg of nanosheet was added in 15 mL of aqueous 20 vol% methanol solution. The photocatalytic reactions were performed under illumination of monochromatic light (270 nm). The total light intensities were 0.89 $mW\,s^{-1}$ (270 nm), and the irradiation area was around 2.25 cm^2. The co-catalysts (0.1 wt.%) were photodeposited in the same reaction solution containing $RhCl_3{\cdot}3H_2O$.

Received: June 27, 2014
Revised: August 17, 2014
Published online: October 9, 2014

Keywords: nanosheets · photocatalysts · photoluminescence · quenching · water splitting

[1] M. A. Baldo, D. F. O'Brien, Y. You, A. Shoustikov, S. Sibley, M. E. Thompson, S. R. Forrest, *Nature* **1998**, *395*, 151–154.
[2] A. Kudo, Y. Miseki, *Chem. Soc. Rev.* **2009**, *38*, 253–278.
[3] O. Lehmann, K. Koempe, M. Haase, *J. Am. Chem. Soc.* **2004**, *126*, 14935.
[4] K. Riwotzki, M. Haase, *J. Phys. Chem. B* **1998**, *102*, 10129–10135.
[5] D. L. Dexter, J. H. Schulman, *J. Chem. Phys.* **1954**, *22*, 1063–1070.
[6] T. Honma, K. Toda, Z.-G. Ye, M. Sato, *J. Phys. Chem. Solids* **1998**, *59*, 1187–1193.

[7] D. Wang, Q. Yin, Y. Li, M. Wang, *J. Lumin.* **2002**, *97*, 1 – 6.
[8] T. Ishihara, H. Nishiguchi, K. Fukamachi, Y. Takita, *J. Phys. Chem. B* **1998**, *103*, 1 – 3.
[9] R. Konta, T. Ishii, H. Kato, A. Kudo, *J. Phys. Chem. B* **2004**, *108*, 8992.
[10] a) Z. Zhang, W. Sigle, F. Phillipp, M. Ruehle, *Science* **2003**, *302*, 846 – 849; b) K. Kimoto, R. J. Xie, Y. Matsui, K. Ishizuka, N. Hirosaki, *Appl. Phys. Lett.* **2009**, 94.
[11] a) R. Ishikawa, A. R. Lupini, S. D. Findlay, T. Taniguchi, S. J. Pennycook, *Nano Lett.* **2014**, *14*, 1903.
[12] a) S. Ida, C. Ogata, M. Eguchi, W. J. Youngblood, T. E. Mallouk, Y. Matsumoto, *J. Am. Chem. Soc.* **2008**, *130*, 7052 – 7059; b) S. Ida, C. Ogata, U. Unal, K. Izawa, T. Inoue, O. Altuntasoglu, Y. Matsumoto, *J. Am. Chem. Soc.* **2007**, *129*, 8956 – 8957; c) T. C. Ozawa, K. Fukuda, K. Akatsuka, Y. Ebina, T. Sasaki, K. Kurashima, K. Kosuda, *J. Phys. Chem. C* **2008**, *112*, 1312 – 1315.
[13] a) R. E. Schaak, T. E. Mallouk, *Chem. Mater.* **2000**, *12*, 3427 – 3434; b) R. E. Schaak, T. E. Mallouk, *Chem. Mater.* **2000**, *12*, 2513 – 2516.
[14] Y. Okamoto, S. Ida, J. Hyodo, H. Hagiwara, T. Ishihara, *J. Am. Chem. Soc.* **2011**, *133*, 18034 – 18037.
[15] K. Toda, T. Teranishi, Z. G. Ye, M. Sato, Y. Hinatsu, *Mater. Res. Bull.* **1999**, *34*, 971 – 982.

